FOURTH EUROPEAN ROTORCRAFT AND POWERED LIFT AIRCRAFT FORUM

Paper No. 27

FREE FEATHERING ROTOR

V.V. UTGOFF

DEPARTMENT OF THE NAVY
UNITED STATES NAVAL ACADEMY
ANNAPOLIS, MARYLAND 21402

September 13 + 15, 1978
STRESA - ITALY

Associazione Italiana di Aeronautica ed Astronautica
Associazione Industrie Aerospaziali

FREE-FEATHERING ROTOR

V. V. Utgoff
Aerospace Engineering Department
U. S. Naval Academy, Annapolis, Maryland, U.S.A.

ABSTRACT

This paper presents preliminary results of an analytic and experimental investigation of a free-feathering rotor.

The free-feathering rotor differs from a conventional fully articulated rotor in that in the free-feathering rotor a flap angle is imposed but the blades are free to rotate about the pitch axis, whereas in the conventional rotor a pitch angle is imposed but the blades are free to flap. Blade pitch in the free-feathering rotor depends on a balance of aerodynamic and centrifugal forces, just as the flap angle depends on this balance in a conventional rotor.

In general, analysis and tests are in fair agreement. In all operating modes the thrust coefficient and coning angle are essentially linearly related if no part of the blade is stalled. In powered axial flow (vertical climb or rotor prop mode) the thrust coefficient decreases with increasing inflow ratio, but to a far lesser degree than in the case of a fixed pitch propeller.

In autorotative vertical descent the thrust coefficient and inflow ratio are substantially independent of rotational speed.

In an in-plane flow field (horizontal flight), the thrust coefficient is essentially independent of advance ratio. The rolling moment coefficient is near zero for advance ratios up to about .5. Above .5 the rolling moment coefficient increases linearly with advance ratio.

NOTATION

A	disc area
C_{D_E}	equivalent drag coefficient, $D_E/\rho A V_{TIP}^2$
CF	centrifugal force
C_L	rolling moment coefficient, $L/\rho A V_{TIP}^2$
C_T	thrust coefficient, $T/\rho A V_{TIP}^2$
D_E	equivalent drag
e	flapping hinge offset
g	gravitational acceleration
L	rolling moment
m	mass
R	rotor radius
r	radial distance
r_I	radial distance to blade mass center
r_o	root radius
T	thrust
v	induced velocity
V	flow velocity, axial or in-plane
W	blade weight
x	chordwise distance from leading edge
x_A	chordwise distance to aerodynamic center
x_I	chordwise distance to mass center
β	flap angle; coning angle
λ	inflow ratio, $(V+v)/V_{TIP}$
μ	advance ratio, V/V_{TIP}
θ	pitch angle

INTRODUCTION

If the mass center of a rotor blade is behind the pitch axis, for any positive flap angle there will be a component of centrifugal force which will tend to increase blade pitch. If the aerodynamic center is also behind the pitch axis a positive angle of attack will produce a negative aerodynamic pitching moment. Thus, in a free-feathering rotor, blade pitch will be determined by a balance between the centrifugal pitching moment and the aerodynamic pitching moment. Collective pitch is therefore governed by the coning angle selected; and cyclic pitch changes can be effected by cyclic variation of the flap angle.

In the analysis which follows only the quasi-static case is considered. The blade is assumed to be rigid and untwisted. Pitch bearing friction is neglected. Aerodynamic forces are determined by classical blade element methods.

ANALYSIS

Thrust and equivalent drag (the torque divided by the radial distance) are assumed to act at the aerodynamic center. From the geometry of Fig. 1, the blade pitching moment due to aerodynamic forces, taken about the pitch axis, is

$$dM_A = -(x_A - x_p)\,[dT \cos\theta + dD_E \sin\theta]$$

Integrating on r,

$$M_A = -(x_A - x_p)\,[T \cos\theta + D_E \sin\theta], \text{ or}$$

$$M_A = -\rho A R^2 \Omega^2 (x_A - x_p)\,[C_T \cos\theta + C_{D_E} \sin\theta]$$

Centrifugal force acts in the plane of rotation radially from the mass center. Its magnitude depends on the mass, the radial distance to the mass center, and the rotational velocity squared. The radial distance of the mass center may be determined by reference to Figs. 2 and 3. It is

$$(r_I - e) \cos\Gamma + e$$

The angle Γ depends on both β and θ, as follows:

$$(r_I - e) \sin\Gamma = (r_I - e) \sin\beta - (x_I - x_p) \sin\theta$$

The component of centrifugal force causing pitching is, from Fig. 2,

$$CF \sin\Gamma$$

and the moment arm is, from Fig. 3,

$$(x_I - x_p) \cos\theta$$

Γ and β are small angles. Making the usual small angle approximations, the centrifugal pitching moment acting on the blade due to a positive flap angle is

$$M_\beta = \frac{W}{g} r_I \Omega^2 (x_I - x_p) \cos\theta \left[\beta - \frac{(x_I - x_p)}{(r_I - e)} \sin\theta\right]$$

Rearranging terms

$$M_\beta = \Omega^2 (x_I - x_p) \cos\theta \frac{W}{g} \beta r_I$$

$$-\Omega^2 (x_I - x_p)^2 \sin\theta \cos\theta \frac{W}{g} \frac{r_I}{r_I - e}$$

There is another pitching moment due to centrifugal force, commonly known as the "tennis racket" moment, which exists at any blade pitch other than zero. This may be derived by reference to Figure 4. Here, the radial distance to the mass element is

$$\frac{r \cos\Gamma + e}{\cos\gamma}$$

The angle γ depends on Γ and θ, thus

$$\tan\gamma = \frac{(x - x_p) \cos\theta}{r \cos\Gamma + e}$$

The component of centrifugal force contributing to the pitching moment is

$$dCF \sin\gamma$$

and the moment arm is

$$(x - x_p) \sin\theta$$

then

$$dM_\theta = -(r \cos\Gamma + e) \tan\gamma \Omega^2 (x - x_p) \sin\theta \, dm$$

and substituting for $\tan\gamma$ from above yields

$$dM_\theta = -\Omega^2 (x - x_p)^2 \cos\theta \sin\theta \, dm$$

Integrating on x and r,

$$M_\theta = -\Omega^2 \sin\theta \cos\theta I_p$$

where

$$I_p = \int_{r_o}^{R} \int_{L.E.}^{T.E.} (x - x_p)^2 \, dm.$$

This is the moment of inertia of the entire blade about the pitch axis.

For quasi-static equilibrium

$$M_A + M_\beta + M_\theta = 0$$

Dividing by $\Omega^2 \cos\theta$ and solving for β yields

$$\beta = \frac{(x_A - x_p)\,\rho\, AR^2\,(C_T + C_{D_E} \tan\theta) + \left[(x_I - x_p)^2 \frac{W}{g} \frac{r_I}{r_I - e} + I_p\right] \sin\theta}{(x_I - x_p)\frac{W}{g} r_I}$$

This equation was derived without regard to whether the rotor was in an axial or in-plane flow field, or whether it was powered or in autorotation. Accordingly, the equation is valid under all these conditions, provided the appropriate relationships among thrust, equivalent drag, and blade pitch are determined.

TEST EQUIPMENT

The experimental investigation was conducted at the U. S. Naval Academy in the subsonic wind tunnel. This tunnel has a test section 60 centimeters high by 75 centimeters wide and is 1 meter long. Air velocities up to 75 meters per second are available in the test section and the tunnel is provided with a six-degree-of-freedom electronic balance.

Table I gives the characteristics of the test rotor. The pitch axis was located at the leading edge. The blades were mounted in ball-bearing pitch bearings. Provision was made to impose a fixed coning angle as required.

TABLE I

Number of blades	2
Blade length	30 centimeters
Blade chord	2.54 centimeters
Airfoil section	0012
Chordwise mass center	.3c
Radial mass center	20 centimeters
Rotor radius	34 centimeters
Flapping hinge offset	2.6 centimeters

The rotor was attached to an electric drive motor capable of providing a maximum of 3000 RPM. For autorotation tests a ball bearing housing could be mounted on the motor shaft in place of the normal coupling. The motor was mounted so that its axis could be rotated 90 degrees for in-plane flow tests.

RESULTS

The rotor was first tested in the hover mode. Figure 5 is a plot of C_T as a function of the coning angle β. It is evident that C_T is linear with β up to tip stall, as indicated by analysis and test, although the slope of the test results is higher than analysis predicts.

Figure 6 presents the computed relationship between the coning angle and collective pitch. This, also, is nearly linear up to tip stall. It is noteworthy that a very small change in coning angle results in a large change in collective pitch.

The rotor was then tested as a rotorprop, that is, in an axial flow field. Figure 7 shows the relationship between C_T and β for selected inflow ratios. The curve for the hover mode is again reproduced, and it is apparent that the shapes of the curves at moderate inflow ratios are generally similar to that obtained in the hover mode, with C_T decreasing as the inflow ratio increases. This effect is clearly evident in Figure 8 where ~~C_T as a function of inflow~~ ratio is plotted for a number of coning angles. The analytic prediction appears at the bottom, calculated for a coning angle of 1.3°. It should be noted that at inflow ratios greater than zero the thrust coefficient becomes zero while the coning angle is still greater than zero. Physically, this results from the fact that the coning angle is the angle between the hub plane and the pitch axis, but the chordwise mass center lies behind the pitch axis. Thus, for a positive blade pitch angle the mass center may lie in the hub plane while the pitch axis is elevated above this plane. The centrifugal pitching moment then vanishes, and this can only occur if the aerodynamic pitching moment is also zero, that is, at that inflow ratio which, for the particular pitch angle, yields zero thrust.

In Figure 9 the variation of C_T with inflow ratio at a coning angle of 2.6° is compared with a fixed pitch rotorprop of the same characteristics. Blade pitch was selected to produce the same C_T for the fixed pitch rotor in hover as the free-feathering rotor and was computed to be 18°. It is evident that the thrust of a fixed pitch rotorprop drops off much more rapidly with increasing axial velocity than is the case of the free-feathering rotor.

The computed variation of collective pitch with inflow ratio is shown in Figure 10 for a coning angle of 1.3°. It can be seen that, as in the

constant speed propeller, collective pitch increases automatically with inflow ratio.

Next, autorotation in axial flow was investigated (windmill mode). The thrust coefficient and the inflow ratio were found to be independent of axial velocity for any particular coning angle. The relationship between C_T and the coning angle was again found to be linear, with a sharp break at the stall. This is illustrated in Figure 11.

This same relationship is illustrated in another form in Figure 12 where the dependence between coning angle and inflow ratio is shown. Once more the linearity and sharp break at the stall are evident.

In Figure 13 axial velocity is plotted as a function of coning angle for two specific values of disc loading. The minimum autorotative descent velocities for two fixed pitch rotors having identical disc loadings have been computed by momentum theory and are also shown. It appears that for minimum autorotative descent velocity the free-feathering rotor would require a negative coning angle. This is not possible. It would seem, therefore, that the minimum descent velocity of a free-feathering rotor must in any case be greater than for a similar fixed pitch rotor.

The final test in this preliminary investigation was of the rotor in an in-plane flow field, that is, in the mode of a helicopter in horizontal flight. The thrust and rolling moment were determined at a constant coning angle and rotational speed for various flow velocities. The results appear in Figures 14 and 15. It may be seen that the thrust coefficient is essentially linear, increasing very slowly with increasing advance ratio.

The rolling moment is negligible up to an advance ratio of about .5, and then increases sharply and reaches a maximum at an advance ratio of .9.

CONCLUSIONS

The free-feathering rotor appears to be an interesting variant of the conventional free flapping rotor, particularly in rotorprop, propeller, or tail rotor applications. Further investigation of its properties in an in-plane flow field, and an analysis of its dynamic characteristics are required. The results of these investigations will be reported in a subsequent paper.

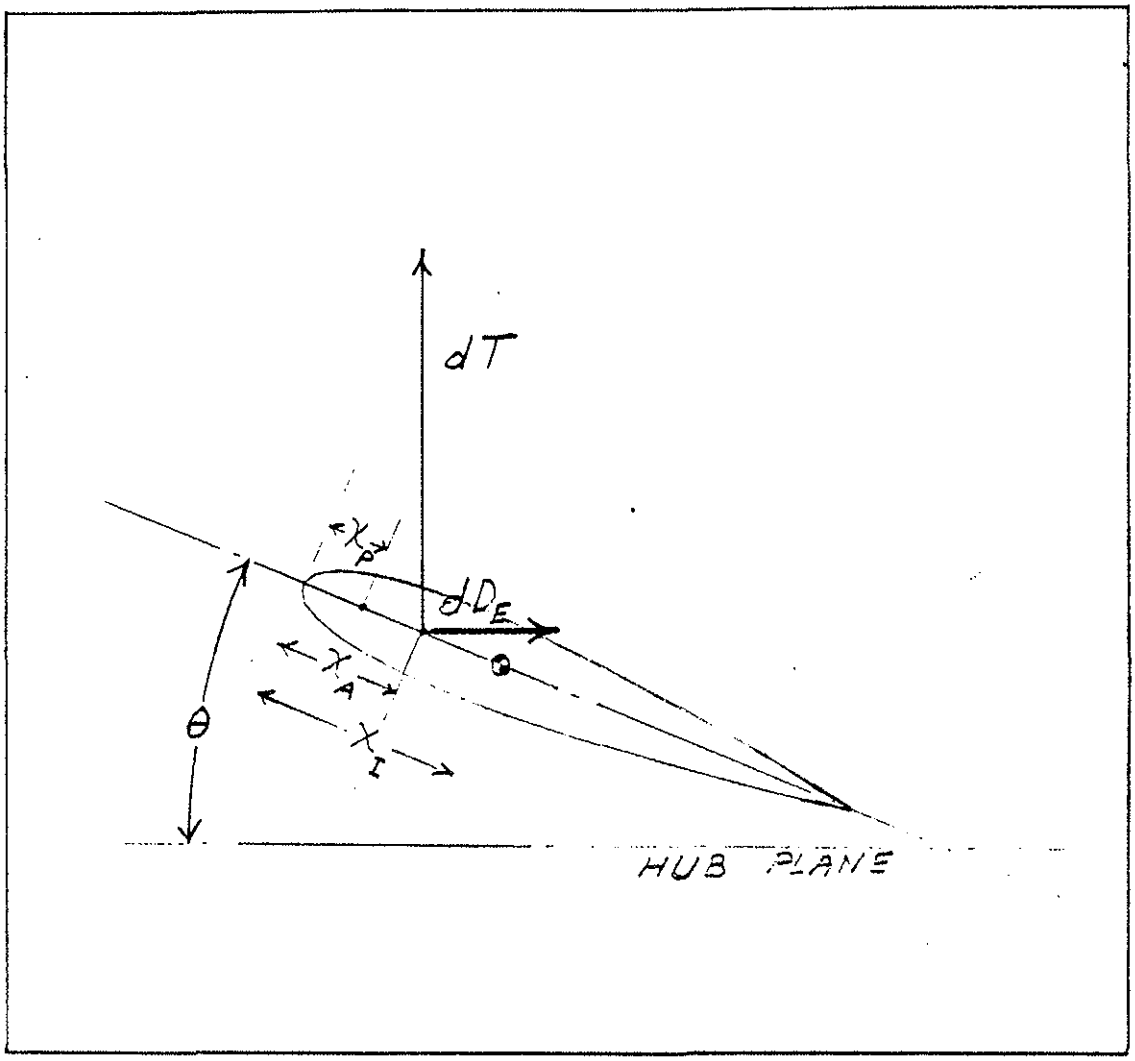

Fig. 1
Blade Element Aerodynamic Forces

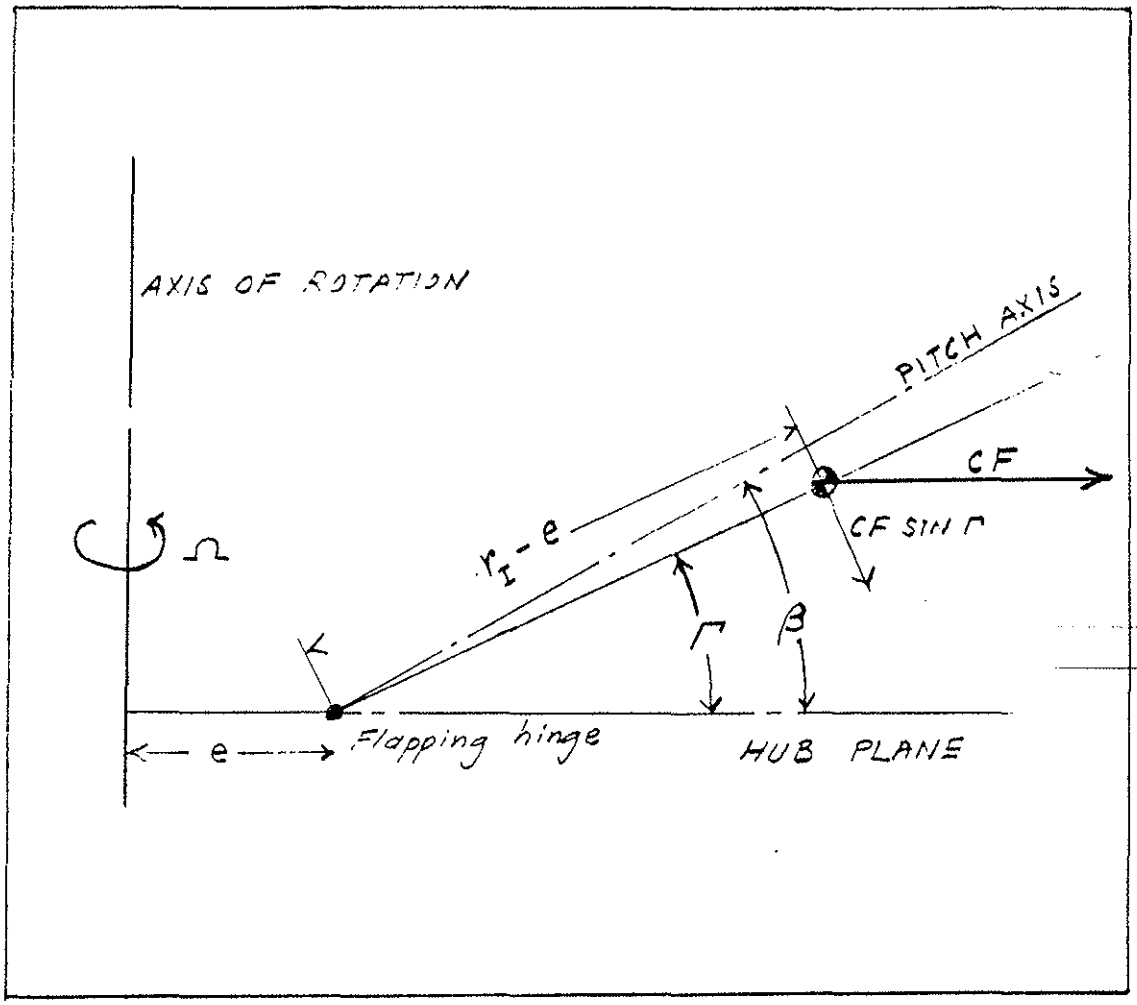

Fig. 2
Blade Side View

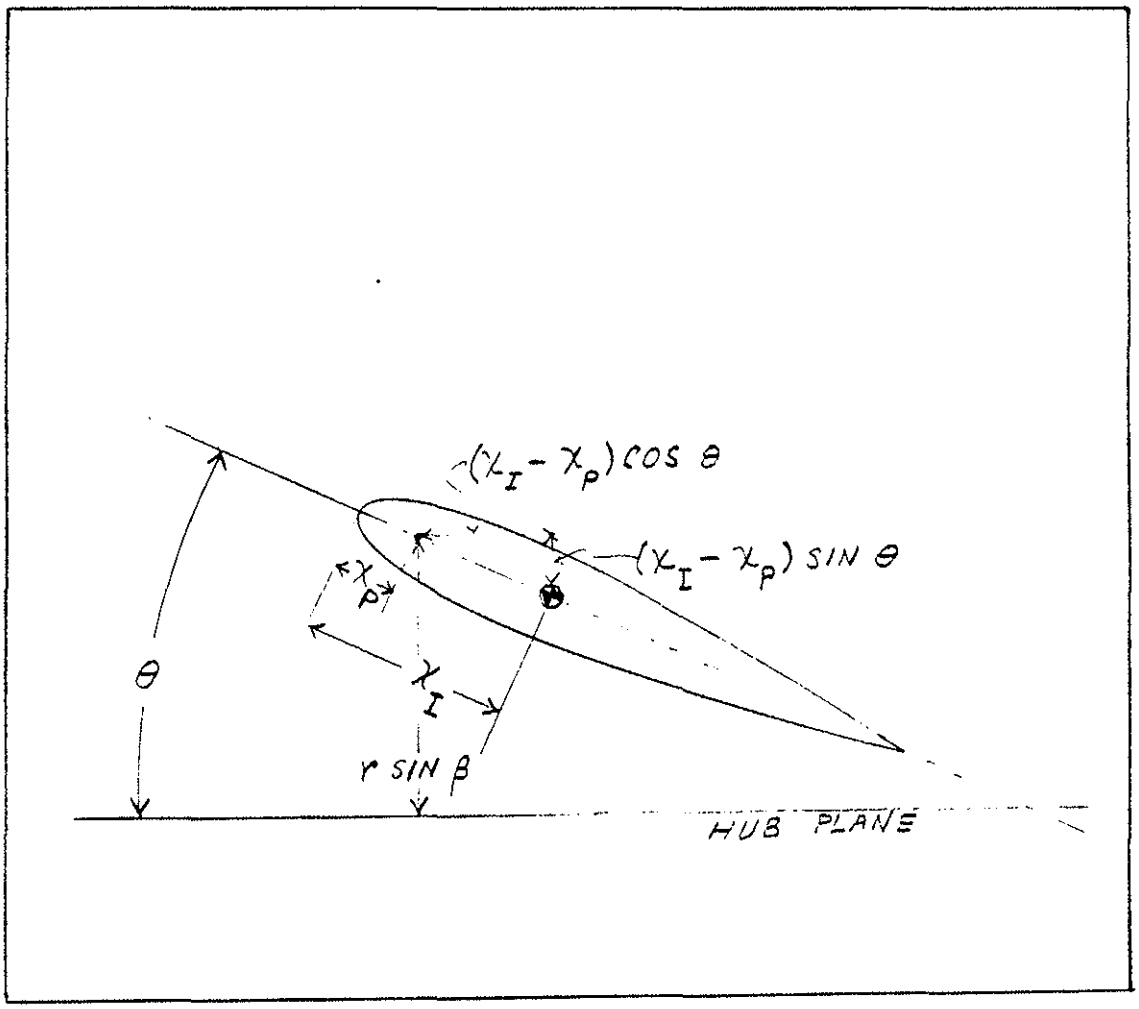

Fig. 3
Blade Element Geometry

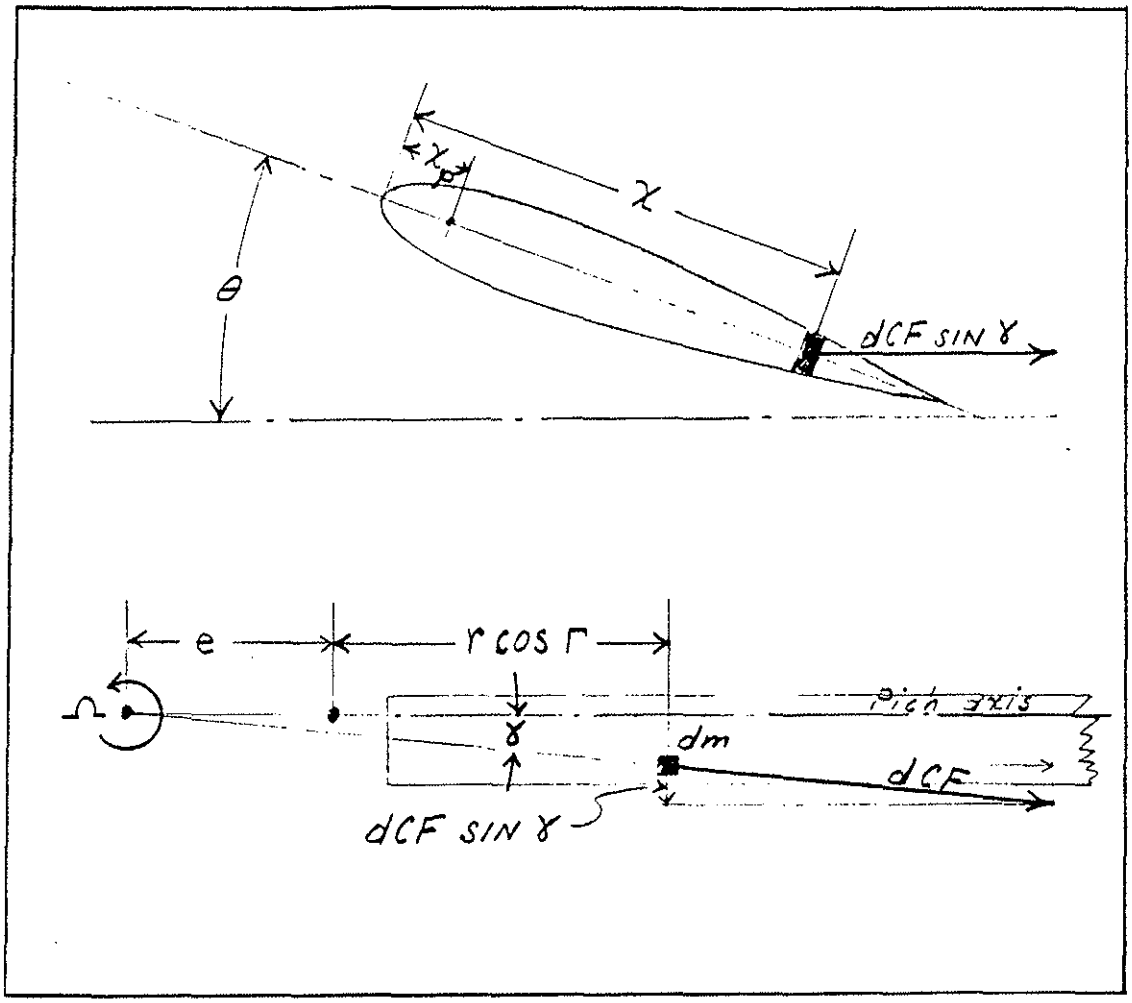

Fig. 4
"Tennis Racket" Moment

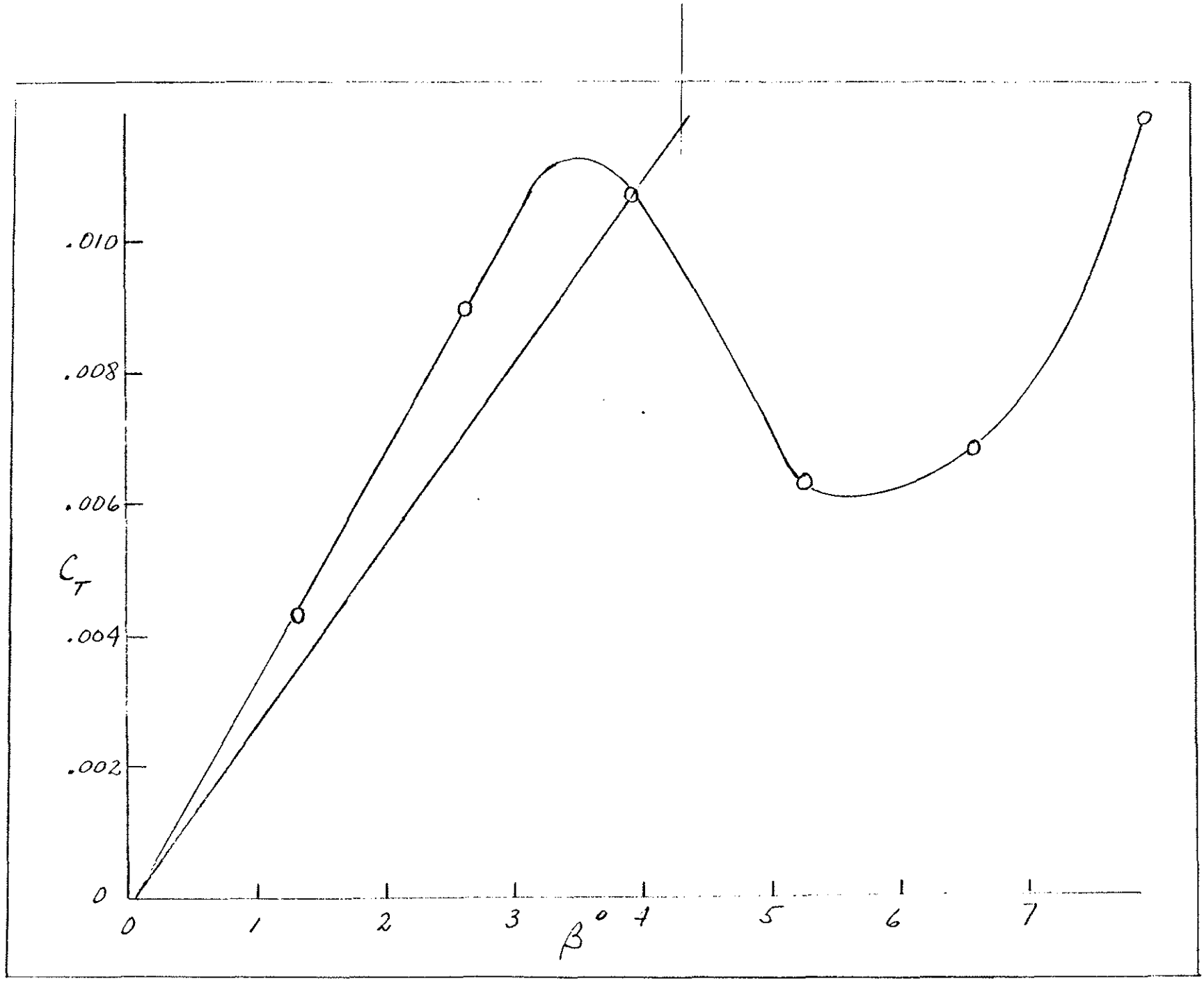

Fi
Thrust Coefficient Dependence on Coning Angle, Hover Mode

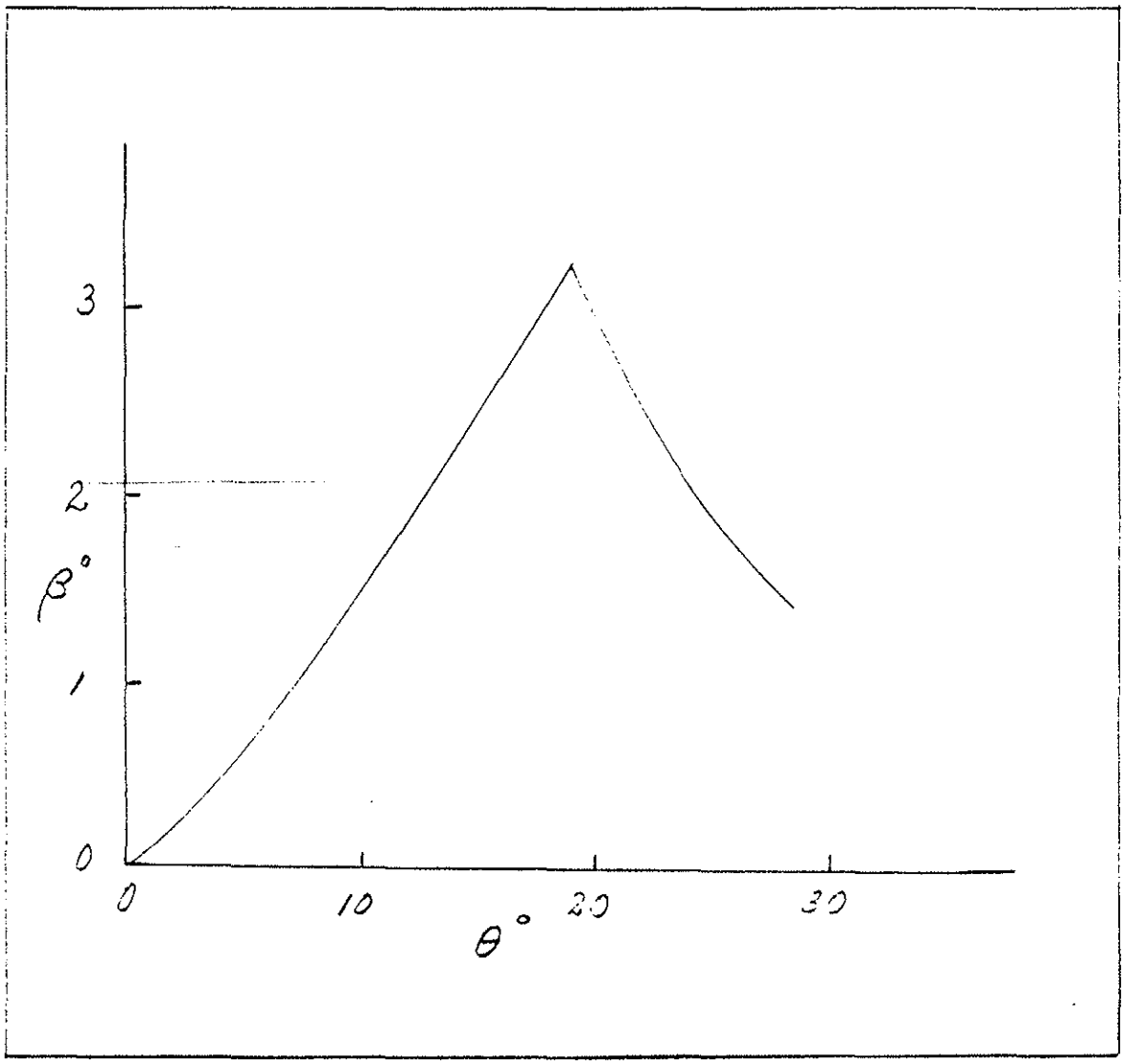

Fig. 6
Computed Collective Pitch Dependence on Coning Angle, Hover Mode

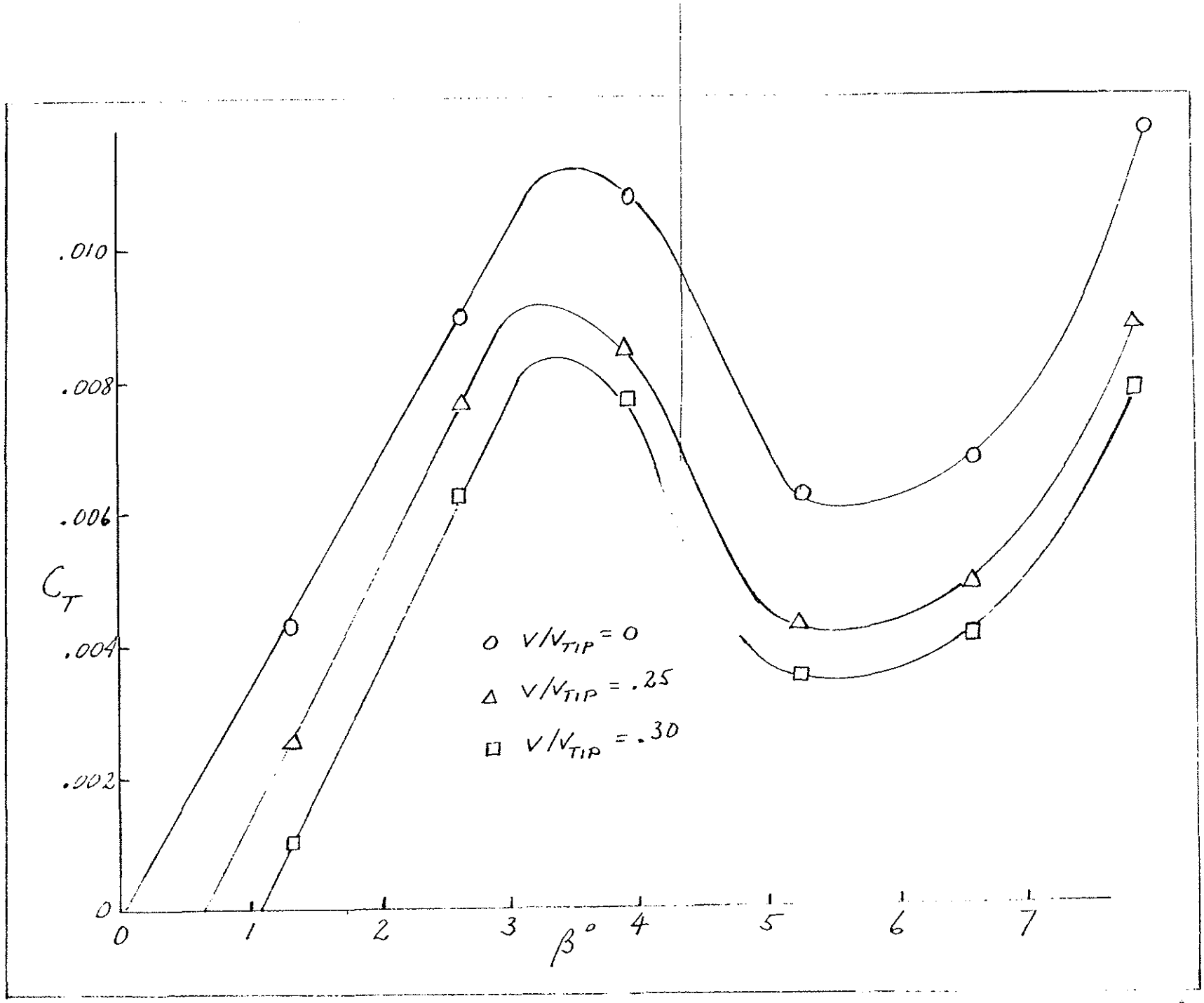

Fig. .
Thrust Coefficient Dependence on Coning Angle, Rotorprop Mode

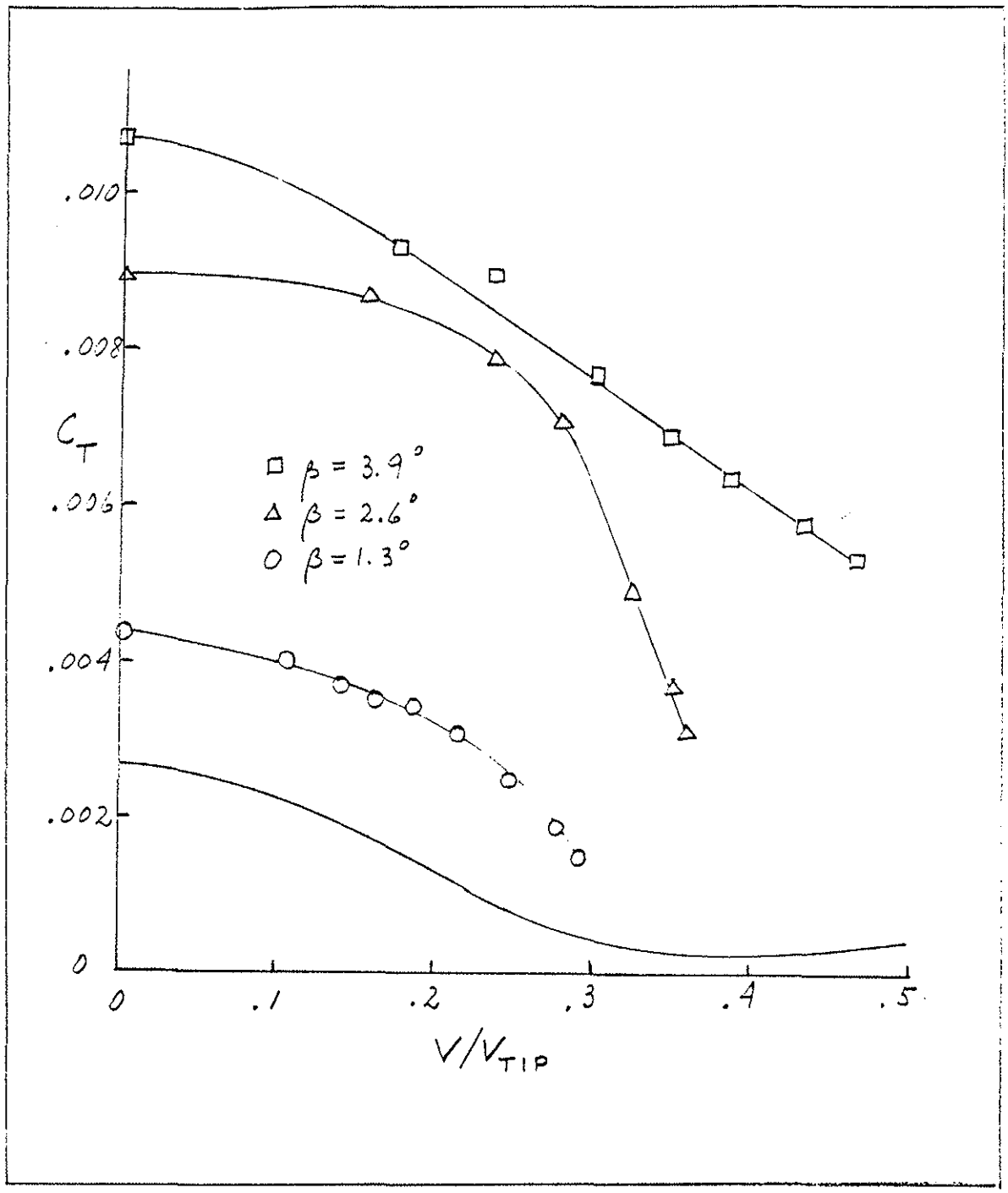

Fig. 8
Thrust Coefficient as a Function of Inflow Ratio, Rotorprop Mode

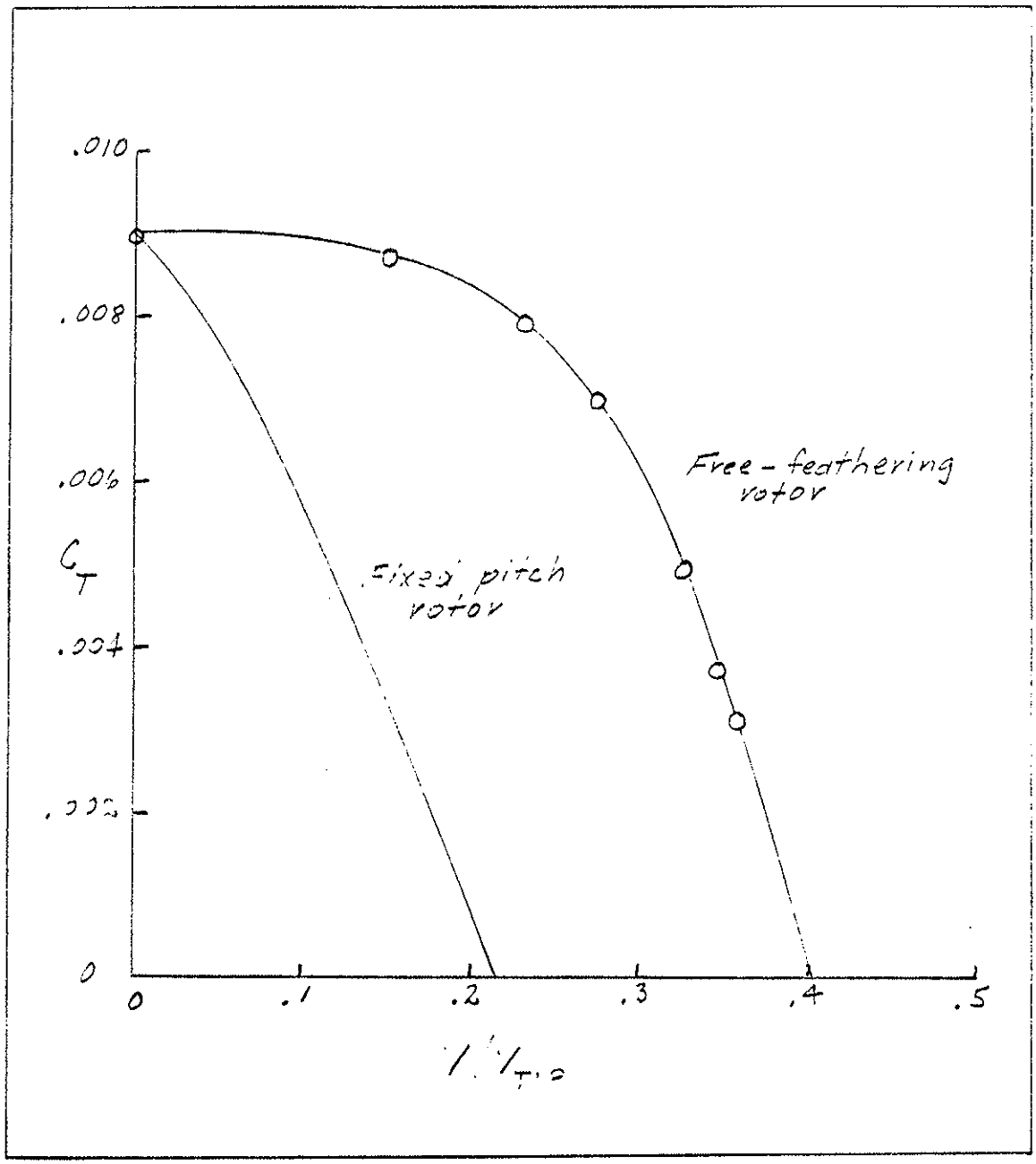

Fig. 9
Free-Feathering Rotor and Fixed Pitch Rotor Compared

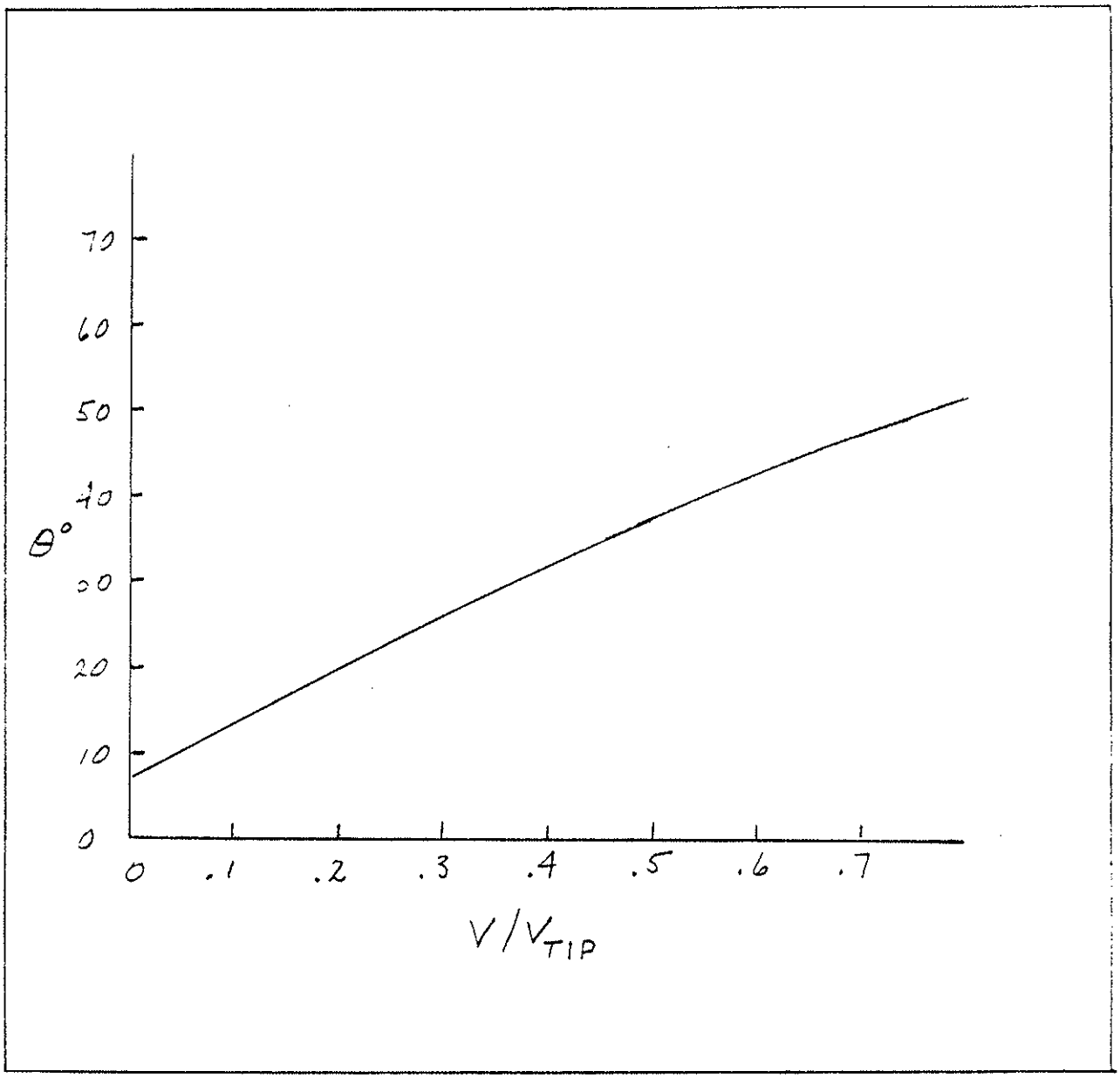

Fig. 10
Computed Collective Pitch Dependence on Inflow Ratio, Rotorprop Mode

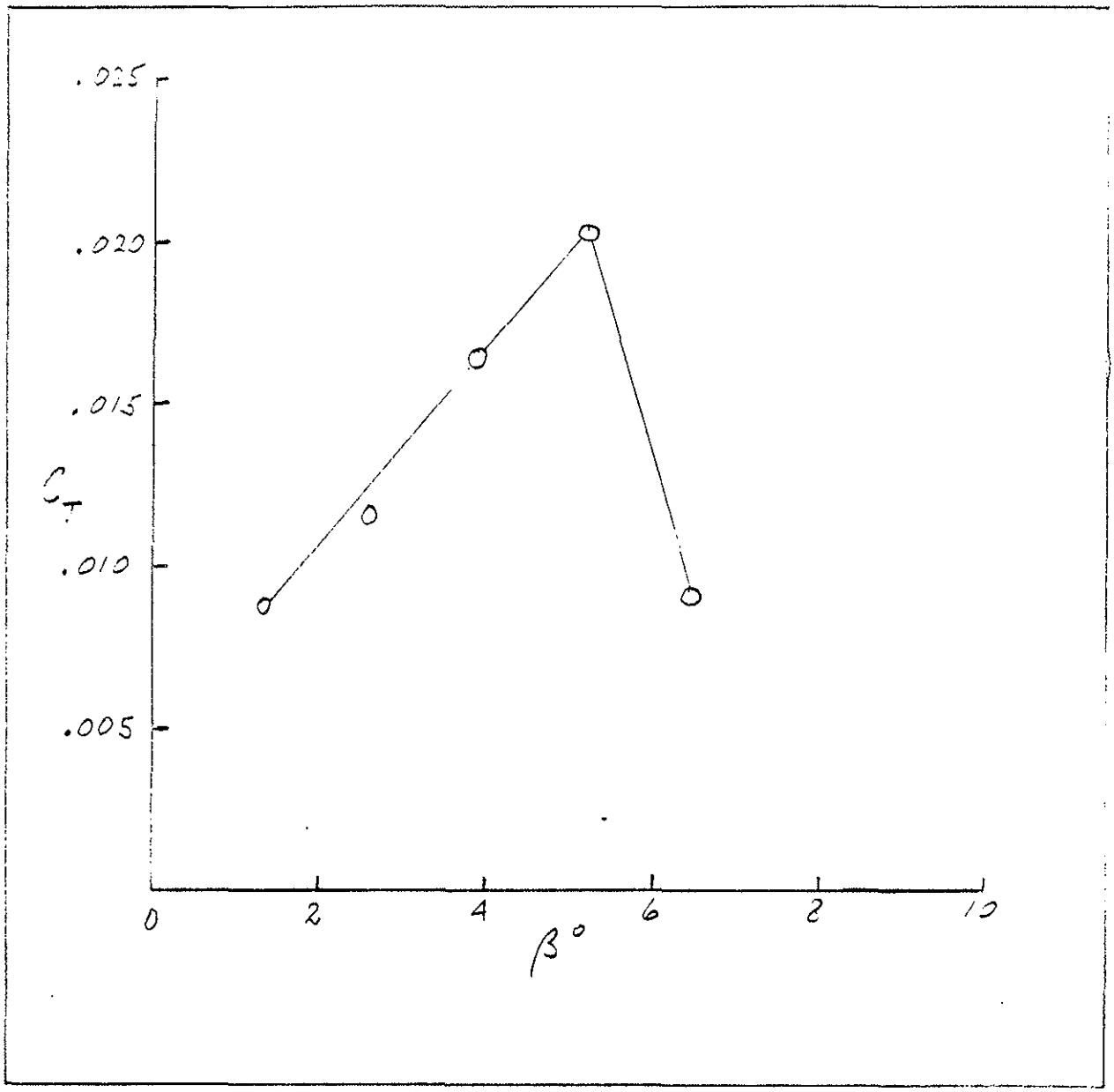

Fig. 11
Thrust Coefficient Dependence on Coning Angle, Windmill Mode

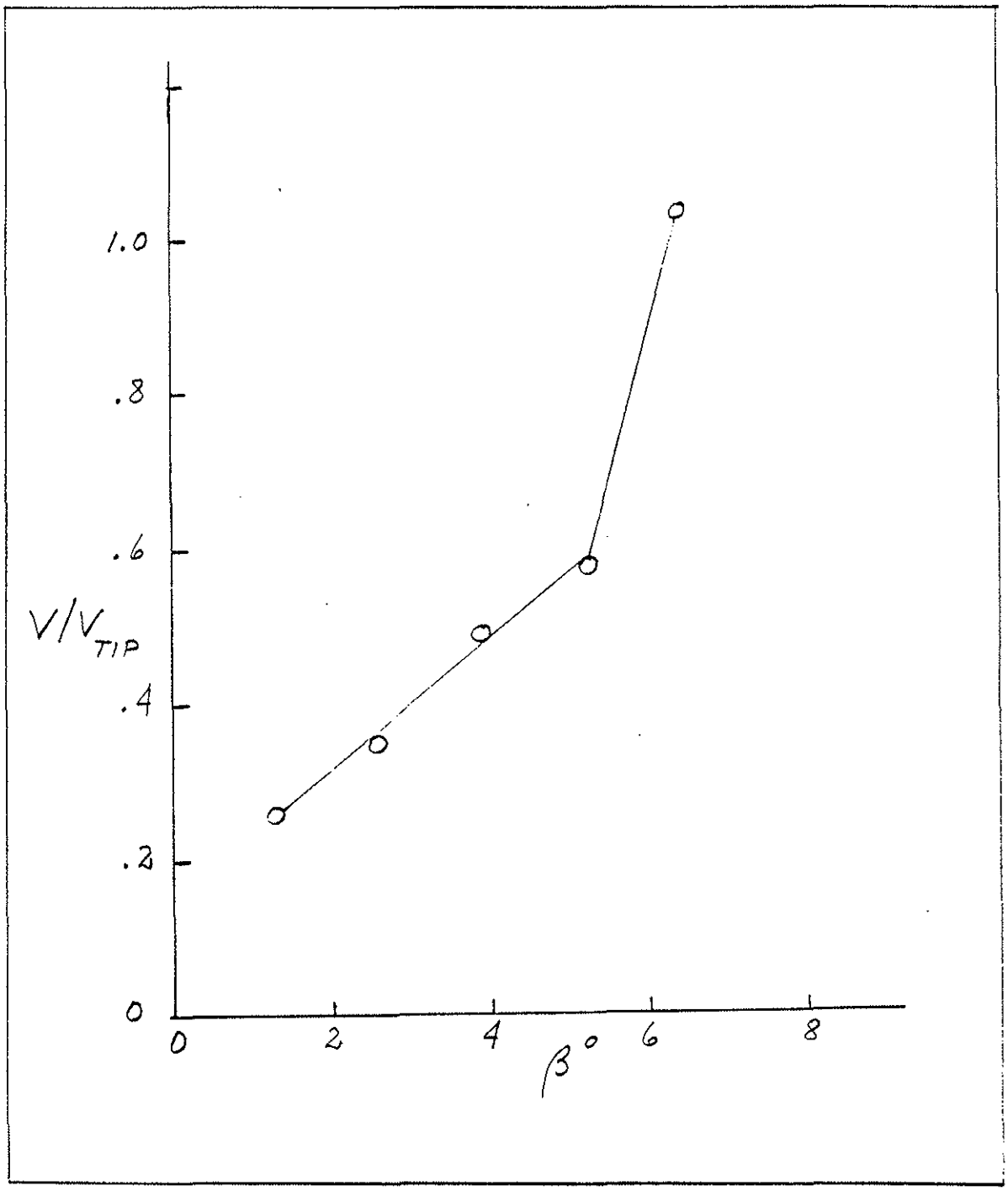

Fig. 12
Inflow Ratio Dependence on Coning Angle, Windmill Mode

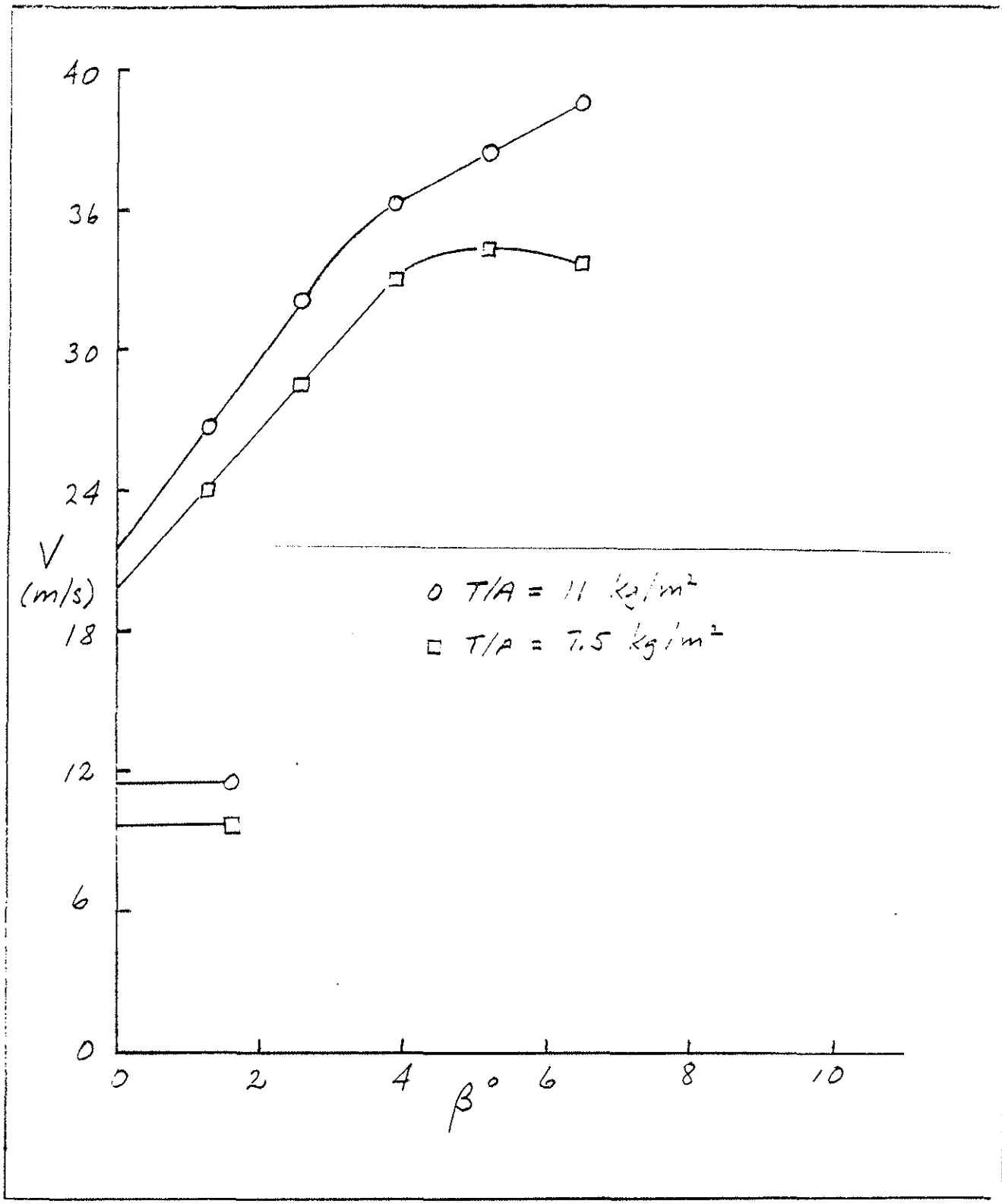

Fig. 13
Autorotative Descent Velocity as a Function of Coning Angle

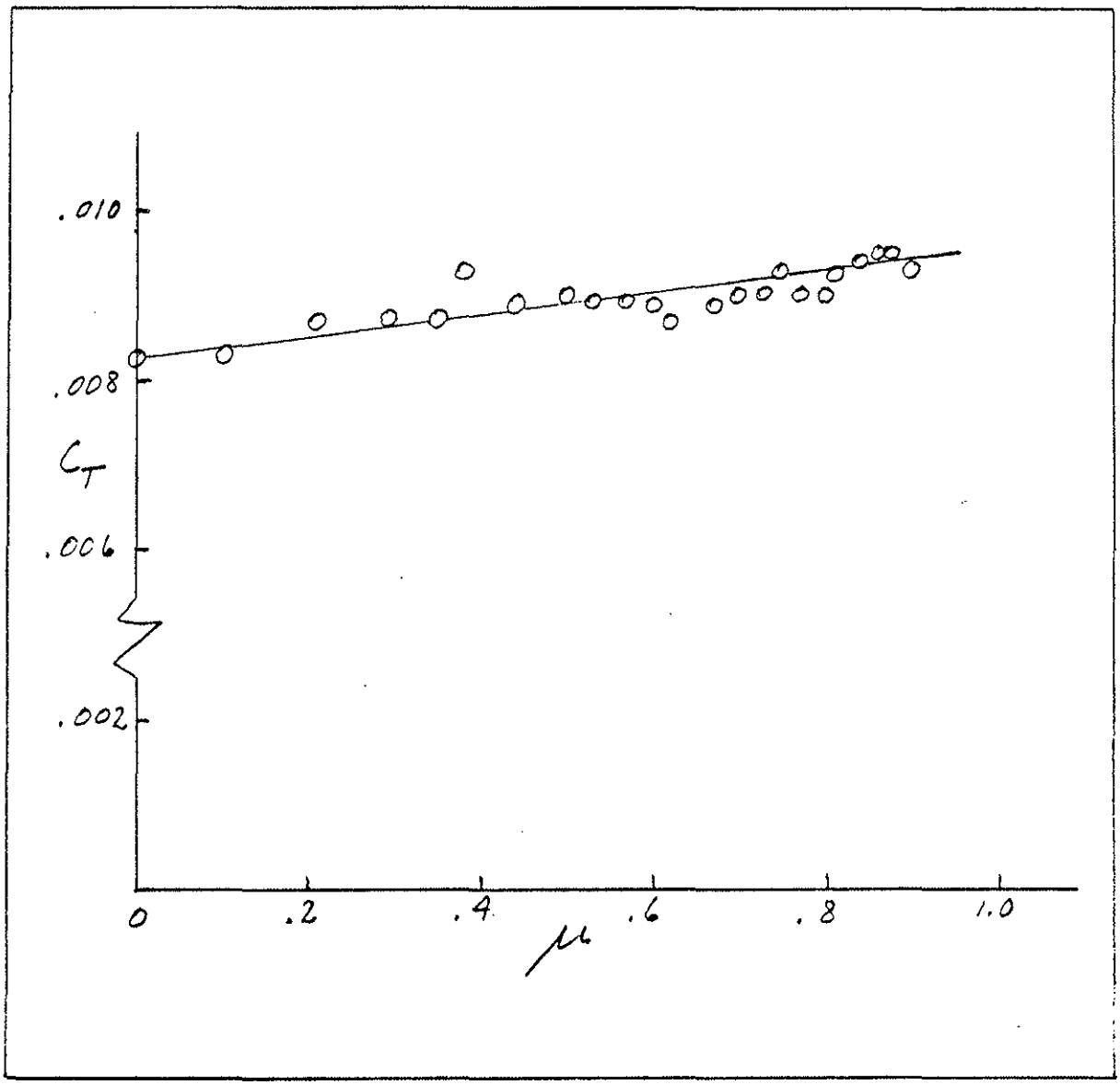

Fig. 14
Thrust Coefficient as a Function of Advance Ratio

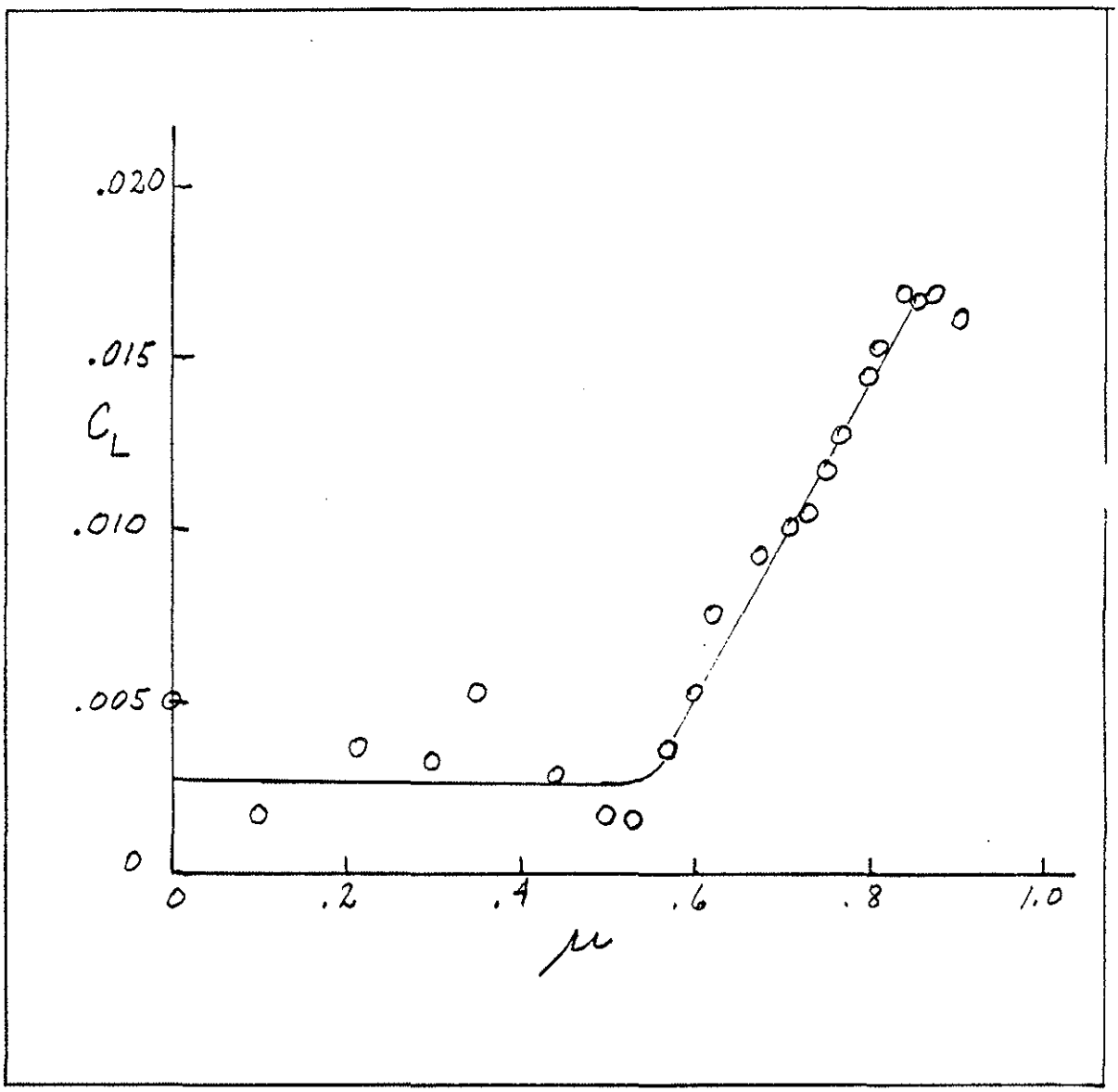

Fig. 15
Rolling Moment Coefficient as a Function of Advance Ratio